ChemPubSoc Europe

DOI: 10.1002/cssc.201500024

CHEMSUSCHEM Full Papers

Facile Synthesis and Enhanced Visible-Light Photocatalysis of Graphitic Carbon Nitride Composite Semiconductors

Huiquan Li,[a, b] Yuxing Liu,[a] Xing Gao,[b] Cong Fu,[b] and Xinchen Wang*[a]

The semiconductor heterojunction has been an effective architecture to enhance photocatalytic activity by promoting photogenerated charge separation. Here, graphitic carbon nitride (CN) and B-modified graphitic carbon nitride (CNB) composite semiconductors were fabricated by a facile calcination process using cheap, sustainable, and easily available sodium tetraphenylboron and urea as precursors. The synthetic CN-CNB-25 semiconductor with a suitable CNB content showed the highest visible-light activity. Its degradation ratio for methyl orange and phenol was more than twice that of CN and CNB and its H_2 evolution rate was ~3.4 and ~1.8 times higher than that of CN and CNB, respectively. It also displayed excellent stability and reusability. The enhanced activity of CN-CNB-25 was attributed predominantly to the efficient separation of photoinduced electrons and holes. This paper describes a visible-light-responsive CN composite semiconductor with great potential in environmental and energy applications.

Introduction

Photocatalysis has attracted widespread interest because of its potential applications in energy production and environmental protection.[1] The photocatalytic activity of a semiconductor depends on its surface area, particle size, morphology, band position, band gap, etc.[2] To date, most studies have concentrated on metal oxides, metal nitrides, and metal sulfides as semiconductor photocatalysts,[3] but these photocatalysts have been restricted by low efficiency as a result of the fast recombination rate of photogenerated electron–hole pairs.[4] Recently, a cheap, easily available, graphitic carbon nitride semiconductor that has controllable band gaps, suitable band positions, and high thermal and chemical stability has been introduced as a photocatalyst for water splitting, organic photosynthesis, and pollutant degradation.[5] However, this π-conjugated carbon nitride framework is also limited by fast charge recombination and slow charge mobility.[6]

Many studies have shown that the construction of heterojunctions between two semiconductors, such as graphitic carbon nitride (CN)/TaON,[7] CN/Bi_2WO_6,[8] CN/Ag_3PO_4,[9] NiO/TiO_2,[10] $GaFe_2O_4$/$PbBi_2Nb_{1.9}W_{0.1}O_9$,[11] SnO_2/ZnO,[12] and ZnO/ZnSe,[13] can enhance the separation efficiency of photoinduced electrons and holes at the heterojunction of composites to enhance photocatalytic activities.[2c] Recently, Zhang and coworkers[2c] reported that CN/sulfur-mediated graphitic carbon nitride (CN/CNS) isotype heterojunctions synthesized by an approach based on the band alignment between CN and CNS had an enhanced charge separation efficiency, which arises from the band offsets and results in a clear improvement in the photocatalytic H_2 evolution performance. Lin et al.[4d] reported that B-modified graphitic carbon nitride (CNB) narrows the band gap of CN and improves its ability to harvest visible light, which enhances its photocatalytic H_2 evolution activity. Hence, a CN-CNB composite semiconductor may be an ideal system to increase visible-light absorption and enhance the separation efficiency of photogenerated charge carriers to achieve a high photocatalytic activity.

Here, CN-CNB composite semiconductors were fabricated by a facile calcination method. Briefly, CNB was synthesized by mixing 10 g urea and 6.0 mg sodium tetraphenylboron (Ph_4BNa) in 15 mL deionized water with stirring at 80 °C to remove deionized water, and the resultant solid was calcined at 550 °C for 2.0 h. Then, 10 g urea and a certain amount of CNB were mixed, followed by calcination at 550 °C for 2.0 h. For simplicity, the resulting yellow samples are denoted as CN-CNB-*x*, in which *x* (10, 25, and 50) is the weight-in amount of CNB (10, 25, and 50 mg). The texture, chemical structure, and surface morphology of the CN-CNB samples were characterized by various physical and chemical techniques. The visible-light active CN and CNB photocatalysts were used to fabricate CN-CNB isotype semiconductors, and CN-CNB was designed to reduce the recombination of photoinduced electrons and holes in CN and CNB simultaneously. This would enhance the photocatalytic H_2 evolution activity from water splitting and improve the degradation efficiency for methyl orange and phenol, which are hazardous models used commonly to evaluate the degradation capability of catalysts under visible-light

[a] H. Li, Y. Liu, Prof. X. Wang
State Key Laboratory of Photocatalysis on Energy and Environment
School of Chemistry and Chemical Engineering
Fuzhou University
Fuzhou 350002 (PR China)
E-mail: xcwang@fzu.edu.cn
Homepage: http://wanglab.fzu.edu.cn

[b] H. Li, X. Gao, C. Fu
School of Chemistry and Materials Engineering
Fuyang Normal College
Fuyang 236037 (PR China)

Supporting Information for this article is available on the WWW under http://dx.doi.org/10.1002/cssc.201500024.

($\lambda > 420$ nm) irradiation. Furthermore, details of the photocatalytic mechanism are discussed in this work.

Results and Discussion

The XRD patterns of CN, CNB, CN-CNB-10, CN-CNB-25, and CN-CNB-50 are shown in Figure 1a. The patterns of all of the samples have two distinct peaks at $2\theta = 13.0$ and 27.4°, which correspond to an in-plane repeating motif and the stacking of the CN-conjugated layers along the (002) direction, respectively.[6c,14] The structures and functional groups of CN, CNB, CN-CNB-10, CN-CNB-25, and CN-CNB-50 were confirmed by FTIR spectroscopy. The FTIR spectra of all samples show similar characteristic bands of aromatic CN heterocycles at $\tilde{\nu} = 1200$–1600 cm^{-1} and tri-*s*-triazine units at $\tilde{\nu} = 800$ cm^{-1} (Figure 1b).[15] However, in the CNB and CN-CNB composites, vibrations of the B-related group (N–B–N) are hardly seen, which may be attributed to the overlap of the band with that of the C–N vibrations.

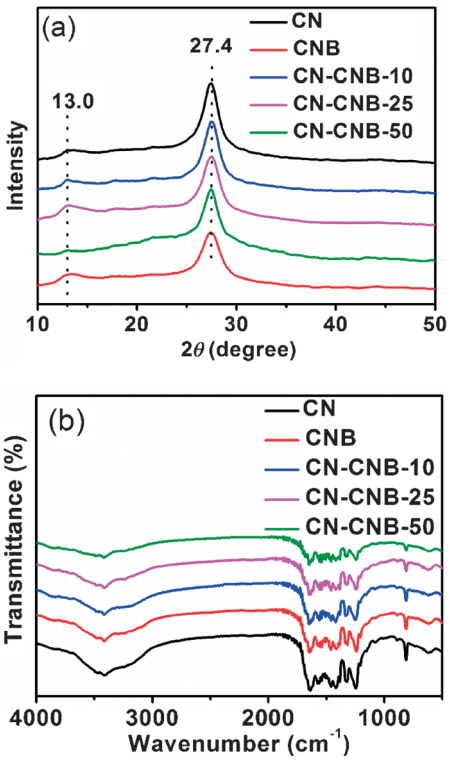

Figure 1. (a) Powder XRD patterns and (b) FTIR spectra of CN, CNB, and CN-CNB composites.

The N_2 adsorption–desorption isotherms of CN, CNB, and CN-CNB-25 are shown in Figure S1. All of the isotherms are of type IV, which is usually associated with capillary condensation in mesopores.[16] The BET surface area, pore volume, and average pore size of CN, CNB, CN-CNB-10, CN-CNB-25, and CN-CNB-50 are listed in Table S1. The BET surface area of CN-CNB-10 is 113 $m^2 g^{-1}$, which is higher than that of CN, CNB, CN-CNB-25, and CN-CNB-50 at 46, 101, 77, and 72 $m^2 g^{-1}$, respectively. The pore size of the samples is estimated by using the Barrett–Joyner–Halenda (BJH) method, and the pore diameters of CN, CNB, CN-CNB-10, CN-CNB-25, and CN-CNB-50 are approximately 27, 26, 28, 27, and 26 nm, respectively. The pore volume of CN-CNB-10 is 0.67 $cm^3 g^{-1}$, which is larger than that of CN, CNB, CN-CNB-25, and CN-CNB-50 at 0.22, 0.61, 0.45, and 0.34 $cm^3 g^{-1}$, respectively. The high BET surface area and pore volume are likely to contribute to the enhancement of the photocatalytic activity.

The formation of the heterostructure between CN and CNB is demonstrated clearly by the TEM images (Figure 2). A typical layered platelet-like surface morphology (Figure 2a) and a thin, silk-like nanostructure (Figure 2b) are identified for CN and CNB, respectively.[4d] CNB is packed closely onto CN, both of which are integrated together as a heterostructure, and CNB is grafted on the surface of CN, which results in the CN-CNB hybrid (Figure 2c and d). These heterostructures were characterized by high-resolution X-ray photoelectron spectroscopy (XPS) for C 1s and N 1s. The binding energies (BEs) of peaks centered at 288.1 and 398.6 eV for C 1s and N 1s, respectively, of CN-CNB-25 are higher than those of CN and CNB, which can be attributed to the strong interaction between CN and CNB or the formation of CN-CNB heterojunctions (Figure 3).[17] In addition, a clear B 1s XPS peak with a BE of ~191.6 eV was observed for the CNB and CN-CNB-25 samples (Figure S2), which corresponds to N–B–N coordination.[18] This implies that some boron atoms are introduced into the carbon sites of the CN matrix.

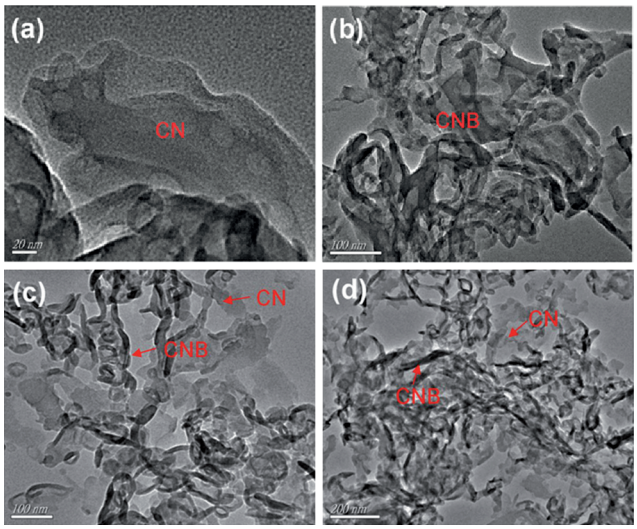

Figure 2. TEM images of (a) CN, (b) CNB, and (c, d) CN-CNB-25.

EPR spectra of CN, CNB, and CN-CNB-25 are displayed in Figure 4a. A Lorentzian line centered at $g = 2.0034$ is observed, which implies the generation of unpaired electrons on π-conjugated CN aromatic rings.[14a,19] This Lorentzian line is enhanced after the formation of the CN-CNB heterostructure (Figure 4a), presumably because of the redistribution of π electrons within the CN-CNB heterojunction through band offsets. Therefore, the formation of the CN-CNB heterostructure is

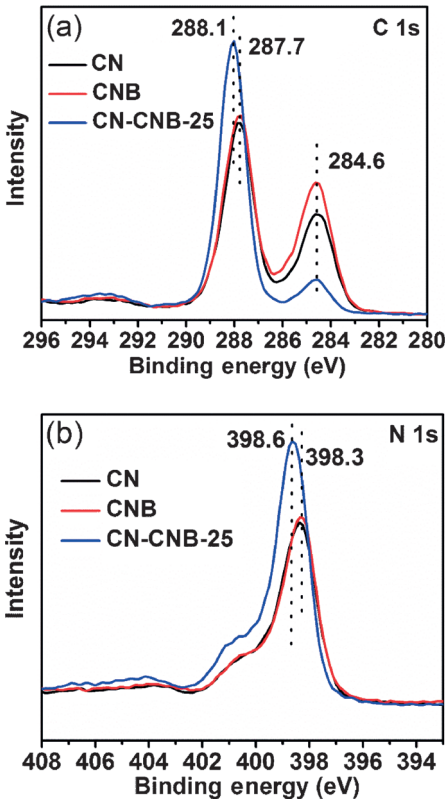

Figure 3. High-resolution XPS spectra of the (a) C 1s and (b) N 1s core levels of CN, CNB, and CN-CNB-25.

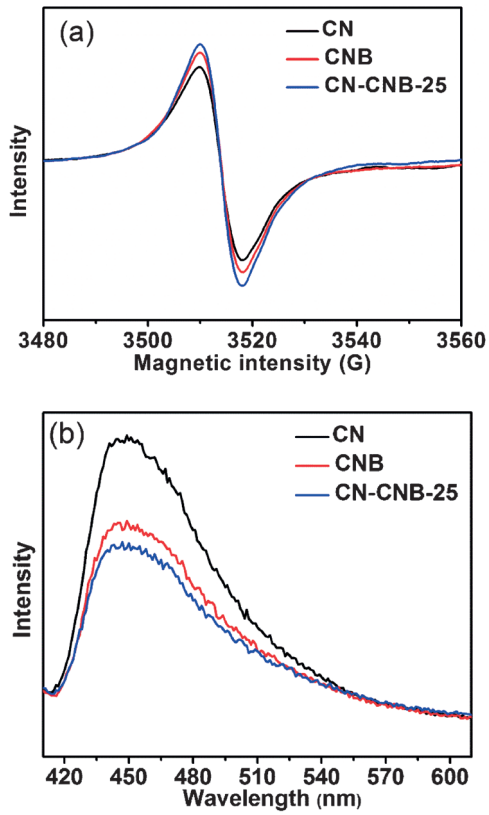

Figure 4. (a) EPR and (b) PL spectra of CN, CNB, and CN-CNB-25.

useful to optimize the electronic band structure for charge migration and separation.

Photoluminescence (PL) emission spectroscopy can be used to characterize heterostructures by revealing the transfer and separation efficiency of photoinduced charge carriers.[6c,12,13,20,21] The PL emission spectra of CN, CNB, and CN-CNB-25 were measured at room temperature with an excitation wavelength of 400 nm (Figure 4b). A strong PL emission peak is observed for the pristine CN, which can be attributed to the radiative recombination of charge carriers. Compared with CN and CNB, the emission peak position of the CN-CNB-25 composite is hardly changed, but its relative intensity is lower. This suggests that the separation efficiency of the photogenerated electrons and holes can be improved by the band offsets in the CN-CNB heterojunction.

CN, CNB, and CN-CNB-25 were evaluated by electrochemical impedance spectroscopy (EIS; Figure 5a) and photocurrent

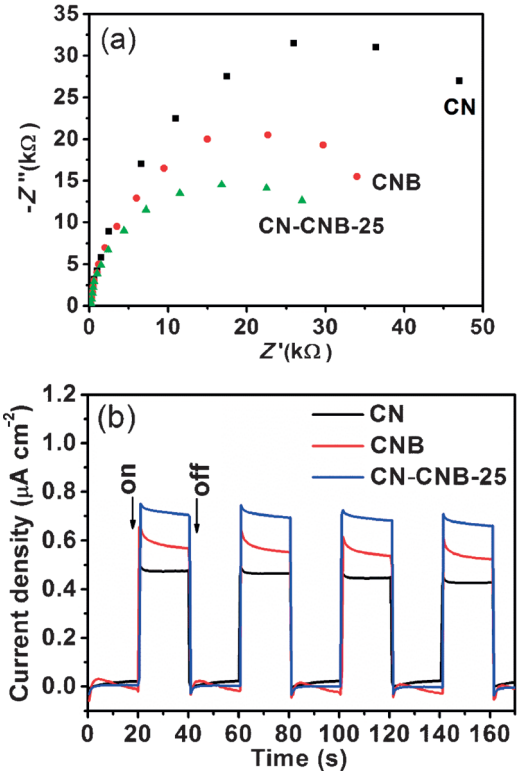

Figure 5. Photo-electrochemical properties of CN, CNB, and CN-CNB-25 in a 0.1 M Na_2SO_4 aqueous solution (pH 6.8) under visible-light irradiation ($\lambda > 420$ nm). (a) EIS Nyquist plots at −0.1 V bias potential vs. Ag/AgCl and (b) the periodic on/off photocurrent response at −0.2 V bias potential vs. Ag/AgCl.

tests (Figure 5b). A clear decrease in the diameter of the Nyquist plot for CN-CNB-25 is observed (Figure 5a), which implies that the electronic resistance of CN-CNB-25 is smaller than that of CN and CNB.[22] This is also supported by the photocurrent tests shown in Figure 5b. An enhanced photocurrent for CN-CNB-25 is generated, which is 1.5 and 1.2 times higher than that of CN and CNB, respectively, which indicates strongly that

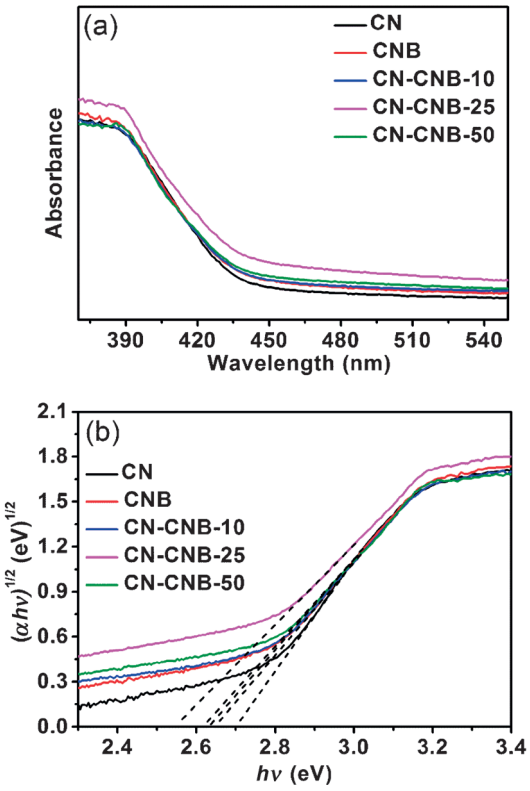

Figure 6. (a) UV/Vis DRS and (b) Kubelka–Munk-transformed reflectance spectra of CN, CNB, and CN-CNB.

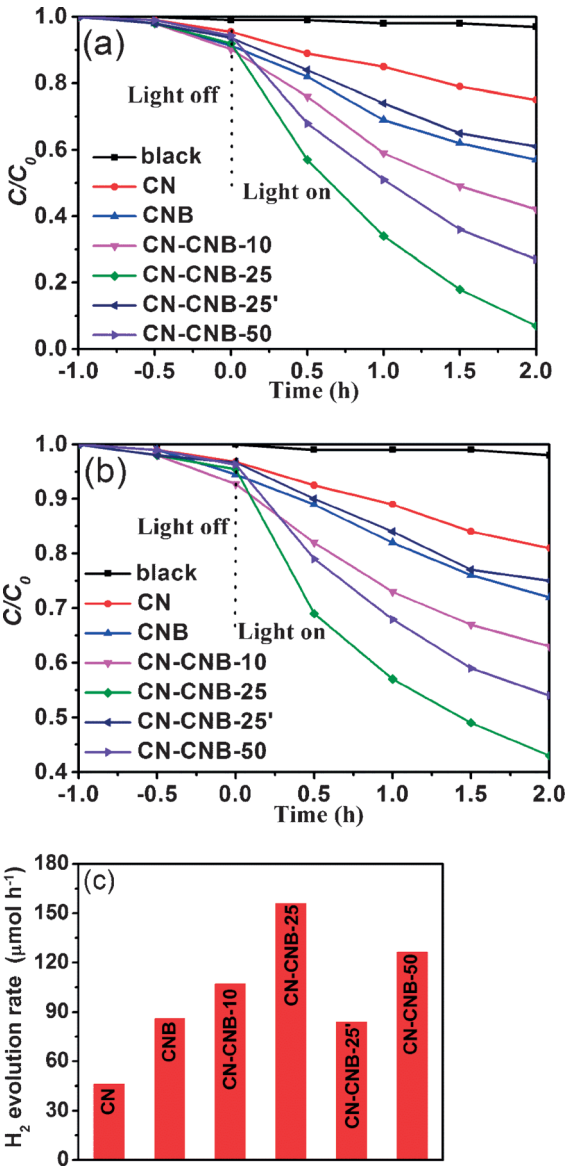

Figure 7. Photodegradation of (a) methyl orange and (b) phenol, and (c) hydrogen evolution rates of CN, CNB, and CN-CNB under visible-light irradiation ($\lambda > 420$ nm).

the mobility of the photoexcited charge carriers is improved.[23] The results show that the separation and migration of the photogenerated charge carriers can be improved by the construction of heterostructures.

The absorbance spectra and Kubelka–Munk-transformed reflectance spectra of CN, CNB, and CN-CNB composites are shown in Figure 6. There is a clear redshift of the absorption of the CNB and CN-CNB composites in comparison with that of CN, and the as-prepared samples show absorption in the visible-light region (Figure 6a). The Kubelka–Munk-transformed reflectance spectra and estimated optical absorption band gaps of CN, CNB, CN-CNB-10, CN-CNB-25, and CN-CNB-50 are shown in Figure 6b. The band gap of CN is 2.70 eV, and the band gaps for CNB, CN-CNB-10, CN-CNB-25, and CN-CNB-50 are estimated to be 2.64, 2.63, 2.55, and 2.62 eV, respectively, which are smaller than that of CN. Thus, the interaction between CN and CNB in the heterojunction may contribute to the narrowing of the band gap because of the modified electronic structures of the photocatalyst matrix, which is in good agreement with the XPS spectra. Interestingly, the band gap of CN-CNB-25 is 0.07 eV lower than that of CN-CNB-50, and the interaction between CN and CNB can contribute to the best photoresponse and the narrowest band gap among the as-prepared samples, although the content of CNB in CN-CNB-50 is higher.

The visible-light photocatalytic activity of the as-prepared CN, CNB, and CN-CNB composite semiconductors was evaluated by the degradation of methyl orange and phenol, which are hazardous models used commonly to test the degradation capability of photocatalysts. If methyl orange or phenol in aqueous solution is irradiated with visible light for 1.0 h in the absence of a photocatalyst, little change in the methyl orange and phenol concentration is observed, which indicates that the self-photodegradation of methyl orange and phenol is negligible (Figure 7a and b). As the CNB content in the CN-CNB composites increases from 0 to 25 mg, the photocatalytic activity of the CN-CNB composites increases and then decreases gradually, and CN-CNB-25 exhibits the highest activity. The photocatalytic activity of CN-CNB-25 is higher than that of CNB and CN. After 2.0 h irradiation, approximately 93% of methyl orange is removed by CN-CNB-25, whereas less than 45% is removed by pure CN and CNB, and approximately 57% of phenol is removed by CN-CNB-25, whereas less than 30% is removed by pure CN and CNB.

The mineralization of methyl orange and phenol in an aqueous solution was also evaluated by monitoring the change of total organic carbon (TOC) in the reaction system using CN-CNB-25 as a representative photocatalyst. The TOC of methyl orange and phenol is degraded by 27.0 and 17.0%, respectively, after visible-light irradiation for 24 h (Figure S3), which shows that the produced organic intermediates continue to decompose into inorganic species. The phenol mineralization rate is slower than that of methyl orange under similar conditions, which may be attributed to the stable chemical structure of phenol.

The photocatalytic H_2 evolution from water splitting over the as-prepared photocatalysts was also studied (Figure 7c). The photocatalytic efficiency for H_2 evolution shows a similar trend to that of methyl orange and phenol degradation with increasing CNB content in the composites. The photocatalytic H_2 evolution rate of CN-CNB-25 is ~3.4 and ~1.8 times higher than that of CN and CNB, respectively.

To underline the necessity of good interconnection for heterojunctions, CN-CNB-25′ mixed mechanically was also tested for photocatalytic activity. The activity of CN-CNB-25′ is clearly lower than that of CN-CNB-25 (Figure 7a–c). Furthermore, our studies show that the photocatalytic activity of CNB-25-CN (in which CN is first formed in CN-CNB composites) is also higher than that of CN and CNB. Its degradation ratio for methyl orange and phenol was more than 2.2 times that of CN and CNB and its H_2 evolution rate was ~4.6 and ~2.5 times higher that of CN and CNB, respectively.

Generally, the spectrum of light absorption, BET surface area, adsorption ability, and efficient charge separation are the four main factors that influence the photocatalytic activity of photocatalysts. The absorption edges of CNB and CN-CNB-10 are comparable (Figure 6a), which means that they possess nearly identical band-gap energies (Figure 6b). In addition, their absorption intensities in the visible-light region are almost the same, which indicates that the two samples produce the same amount of photogenerated electron–hole pairs. However, the photocatalytic activity of CN-CNB-10 is superior to that of CNB (Figure 7a–c). BET surface area and adsorption ability are two notable phenomena (Table S1). First, the CN-CNB-10 sample possesses the highest BET surface area and the best adsorption ability, but its photocatalytic activity is not optimal. Second, both the BET surface area and adsorption ability of CN-CNB-25 and CN-CNB-50 show little difference, but the photocatalytic activity of CN-CNB-25 is much better than that of CN-CNB-50. Based on these two phenomena combined with the results of visible-light absorption, it can be deduced that BET surface area, light absorption, and adsorption ability influence the photocatalytic activity of the CN-CNB composites, but these three aspects are not the most critical factors. Therefore, the enhancement of the photocatalytic activity of the as-prepared CN-CNB composites is mainly because of the efficient charge separation in the intimate CN-CNB heterointerfaces.

The bottom conduction band (CB) and top valence band (VB) potentials (E_{CB} and E_{VB}) of CN are approximately −1.13 and +1.57 eV,[8,24] respectively. Those of CNB are estimated to be −0.87 and +1.77 eV, respectively, according to the empirical equation in the literature.[25] Once CN and CNB are integrated together, the band alignment between the two semiconductors leads to the formation of a type II heterojunction (Figure S4).[26] The CB offset between CN and CNB can drive the migration of photoinduced electrons from CN to CNB, whereas the photogenerated holes (h^+) are transferred from CNB to CN by the VB offset.[26,27] The redistribution of electrons on one side of the junction (CNB) and holes on the opposite side (CN) reduces the recombination of electrons and holes considerably. Moreover, with the successful separation of electron–hole pairs, the lifetime of the photogenerated charge carriers is prolonged efficiently.[21b] A longer lifetime is favorable for fast charge transfer through the interfaces to the surface-adsorbed substrates to promote photoredox reactions. This conclusion is in good agreement with the results of the EPR, PL, EIS, and photocurrent analysis.

This change of visible-light photocatalytic activity over the CN-CNB composite semiconductors may be attributed to two aspects. First, with the increase of CNB content in CN-CNB composites from 10 to 25 mg, a greater contact area between CN and CNB will be formed, which promotes the efficient separation of photogenerated electrons and holes to result in the enhancement of the photocatalytic activity. Second, if the content of CNB increases continuously to excess, excess CNB may decrease the quality of effective heterointerfaces in the CN-CNB, which is unfavorable for the charge transfer at the heterointerfaces. Hence, the photocatalytic activity of the CN-CNB heterojunctions first increases and then decreases with the increasing CNB content, which leads to the excellent photocatalytic activity of CN-CNB-25.

It is well known that $^{\bullet}O_2^-$, h^+, H_2O_2, e^-, and $^{\bullet}OH$ are reactive species for the photocatalytic degradation of organic pollutants.[28] To investigate which of these species are involved in methyl orange and phenol degradation, we conducted experiments with radical scavengers ammonium oxalate (AO), catalase (CAT), isopropanol (IPA), benzoquinone (BQ), and NO_3^-. AO is a scavenger of h^+,[28d] CAT acts as an H_2O_2 scavenger,[28b] IPA is a scavenger of $^{\bullet}OH$ radicals,[28a,b] BQ acts as an $^{\bullet}O_2^-$ radical scavenger,[28a,c] and NO_3^- ions mainly acts as an e^- scavenger.[28e,f] The results are displayed in Figure S5.

The addition of CAT causes a slight change in the photodegradation efficiency of CN-CNB-25. This indicates that H_2O_2 is not a significant active species in the photocatalytic process. After NO_3^- ions are added, the photocatalytic activity of CN-CNB-25 declines slightly, which indicates that e^- also plays a minor role. A significant suppression of photocatalytic activity is seen if BQ, IPA, or AO is added, which confirms the important role of $^{\bullet}O_2^-$, $^{\bullet}OH$, and h^+ in the photodegradation process. Thus, the photocatalytic degradation of methyl orange and phenol is governed mainly by $^{\bullet}O_2^-$, $^{\bullet}OH$, and h^+ rather than by e^- or H_2O_2.

In the current CN-CNB photocatalytic systems, $^{\bullet}O_2^-$ radicals are formed by the reaction of e^- with dissolved O_2. $^{\bullet}OH$ might be generated by direct hole oxidation[29a] or a photogenerated-electron-induced multistep reduction of O_2.[29b] For CN-CNB, the redox potential of the top VB (Figure S4) of CN-CNB was smaller than that of $^{\bullet}OH/OH^-$ [1.99 eV vs. normal hydrogen

electrode (NHE)] and $^{\bullet}OH/H_2O$ (2.27 eV vs. NHE),[23c] which suggests that the photogenerated holes on the surface of CN-CNB were unable to oxidize adsorbed H_2O or OH^- directly to $^{\bullet}OH$. Thus, the $^{\bullet}OH$ formed in the CN-CNB photocatalytic reaction system was principally from the reduction of O_2.

According to the above discussion, the probable reactions that occur in the photodegradation of methyl orange and phenol are shown in Equations (1)–(8):

$$\text{Catalyst (CN-CNB)} + h\nu \rightarrow e^- + h^+ \quad (1)$$

$$e^- + O_2 \rightarrow {}^{\bullet}O_2^- \quad (2)$$

$$e^- + {}^{\bullet}O_2^- + 2H^+ \rightarrow H_2O_2 \quad (3)$$

$$H_2O_2 + e^- \rightarrow {}^{\bullet}OH + OH^- \quad (4)$$

$$H_2O_2 + h\nu \rightarrow 2\,{}^{\bullet}OH \quad (5)$$

$$\text{methyl orange (phenol)} + h^+ \rightarrow \text{products} \quad (6)$$

$$\text{methyl orange (phenol)} + {}^{\bullet}O_2^- \rightarrow \text{products} \quad (7)$$

$$\text{methyl orange (phenol)} + {}^{\bullet}OH \rightarrow \text{products} \quad (8)$$

The stability of the CN-CNB-25 composite during the photocatalytic reaction was investigated by recycling tests (Figure 8). There is no noticeable change in the visible-light photocatalytic activity after four cycles. In addition, through analysis of the XRD patterns of fresh and used CN-CNB-25 (Figure S6), we found that the phase of CN-CNB-25 remains intact after four photocatalytic runs. These results suggest that CN-CNB-25 was not photocorroded during the photocatalytic process and retained good stability, which implies that photocorrosion was inhibited after the CN-CNB heterostructure was constructed. This can be attributed to the high separation and transfer of the photogenerated electron–hole pairs at the heterojunction interfaces between CN and CNB.[30]

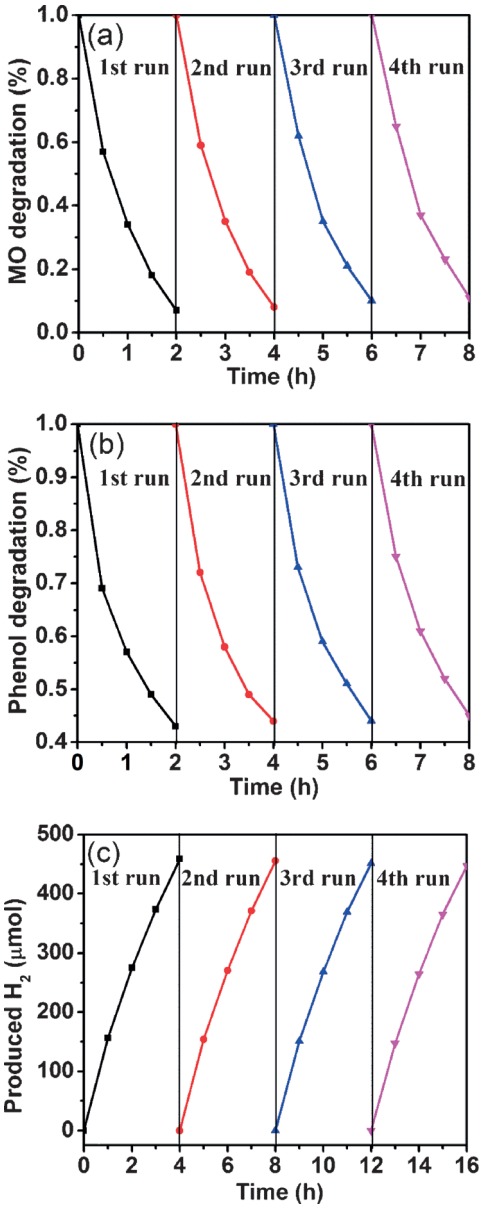

Figure 8. Stability test of a) methyl orange (MO), b) phenol, and c) H_2 photosynthesis (evacuation every 4 h) for CN-CNB-25 under visible-light irradiation ($\lambda > 420$ nm).

Conclusions

We used cheap, sustainable, and easily available sodium tetraphenylboron and urea as precursors to fabricate graphitic carbon nitride (CN) and B-modified graphitic carbon nitride (CNB) composite semiconductor photocatalysts by a facile calcination process. Compared with CNB and CN, the CN-CNB composites exhibited a higher photodegradation efficiency for methyl orange and phenol and a higher photocatalytic H_2 evolution rate from water splitting. This resulted from reduced photogenerated electron–hole recombination caused by the transfer of electrons from CN to CNB and holes from CNB to CN. The CN-CNB-25 composite with an appropriate CNB content exhibited the highest photocatalytic activity, the degradation ratio of which for methyl orange and phenol was more than twice that of CN and CNB. Its H_2 evolution rate was ~3.4 and ~1.8 times higher than that of CN and CNB, respectively, and no noticeable change in activity was observed after four photocatalytic cycles.

Experimental Section

Catalyst preparation

CNB was synthesized by mixing urea (10 g) and Ph_4BNa (6.0 mg) in deionized water (15 mL) with stirring at 80 °C to remove deionized water. The resultant solid was calcined at 550 °C for 2.0 h at a heating rate of 10 °C min^{-1} in air to yield the final sample. CN was obtained following the same procedure. The CN-CNB composites were fabricated by mixing urea (10 g) and different amounts of CNB. The resultant solid was calcined at 550 °C for 2.0 h at a heating rate of 10 °C min^{-1} in air to yield the final samples. For simplicity, the resulting CN-CNB photocatalysts were denoted as CN-CNB-*x*, in which *x* (10, 25, and 50) is the weight-in amount of CNB (10, 25, and 50 mg).

Characterization

XRD data were collected by using a Bruker D8 Advance diffractometer with $CuK_{\alpha 1}$ radiation ($\lambda = 1.5406$ Å). FTIR spectra were recorded by using a Nicolet Magna 670 FTIR spectrometer. Specific surface areas and pore structures were calculated from N_2 adsorption–desorption isotherms at 77 K by using an ASAP2020 HD88 instrument. TEM images were recorded by using a Jeol JEM-2100F microscope. XPS spectra were measured by using a PerkinElmer PHI-1600 ESCA spectrometer using a MgK_{α} X-ray source, and the peak positions were calibrated with respect to the binding energy of the C 1s peak at 284.6 eV. EPR spectra were recorded by using a Bruker model A300 spectrometer. PL spectra were recorded by using a CARY Eclipse (America) fluorescence spectrophotometer at RT with an excitation wavelength of 400 nm. UV/Vis diffuse reflectance spectra (DRS) were measured by using a Varian Cary 500 Scan UV/Vis system. Electrochemical measurements were performed by using a BAS Epsilon Electrochemical System under visible-light irradiation with a conventional three-electrode cell immersed in a 50 mL solution of 0.1 M Na_2SO_4 (pH 6.8). The CN, CNB, and CN-CNB-25 electrodes were used as the working electrodes, which were prepared on indium tin oxide (ITO) conductor glasses. A powder sample (10 mg) was dispersed in DMF (800 μL) with sonication to obtain a slurry mixture. The slurry was spread onto ITO glass, the side of which was protected by Scotch tape. The working electrode was dried overnight under ambient conditions. Uncoated parts of the electrode were isolated by epoxy resin. Pt plate and Ag/AgCl (3 M KCl) electrodes were used as a reference and a counter electrode, respectively. A 300 W Xe lamp with a visible-light band-pass filter ($\lambda > 420$ nm) was employed as the excitation light source.

Photocatalytic activity measurements

The photodegradation efficiency of CN, CNB, and CN-CNB composites was evaluated by the degradation of methyl orange and phenol in an aqueous solution under visible-light irradiation. A 350 W Xe lamp with a 420 nm cut-off filter was used as the visible-light source. Powder catalyst (200 mg) was dispersed into methyl orange or phenol in an aqueous solution (50 mL, 5 mg L^{-1}) for photocatalytic examinations with magnetic stirring. Before visible-light irradiation, the dispersion was kept in the dark for 1.0 h under magnetic stirring to reach an adsorption–desorption equilibrium. Approximately 3.0 mL reactant solution was withdrawn from the reactor periodically, which was centrifuged and analyzed for the degradation of methyl orange or phenol by using a TU-1901 spectrophotometer. Changes of TOC in the CN-CNB-25 reaction system were monitored by using a Shimadzu TOC-L CSH total organic carbon analysis system. Visible-light-induced catalytic hydrogen evolution by CN, CNB, and CN-CNB composites was performed in a Pyrex top-irradiation reaction vessel connected to a closed glass gas-circulation system. H_2 production was performed with a dispersion of powder catalyst (50 mg) in an aqueous solution (100 mL) that contained triethanolamine (10 vol%), and 3 wt% Pt was loaded onto the surface of the catalyst by the in situ photodeposition method using H_2PtCl_6 as the starting material. The reactant solution (pH ≈ 11.1) was evacuated several times to remove air before irradiation. Visible-light irradiation was generated by using a 300 W Xe lamp attached to a 420 nm cut-off filter (intensity: ~332 mW cm^{-2}). During the reaction, the temperature of the reactant solution was maintained at RT by a flow of cooling water. The pH value of the reaction mixture after the photochemical reaction was ~10.8. The evolved gases were analyzed by GC (Shimadzu, GC-8A).

Acknowledgements

This work is financially supported by the National Basic Research Program of China (2013CB632405), the National Natural Science Foundation of China (21425309 and 21173043), the Natural Science Foundation of Higher Education Institutions in Anhui Province of China (KJ2014A191), Postdoctoral Scientific Research Start-up Funding of Fuzhou University in China (601116), College Students' Innovative Training Program of China (AH201410371077), and school-level item (FSB201401003, 2014KJFH01) of Fuyang Normal College of China.

Keywords: boron · carbon · photochemistry · semiconductors · water splitting

[1] a) E. W. McFarland, H. Metiu, *Chem. Rev.* **2013**, *113*, 4391 – 4427; b) J. R. Ran, J. Zhang, J. G. Yu, S. Z. Qiao, *ChemSusChem* **2014**, *7*, 3426 – 3434; c) Z. G. Yi, J. H. Ye, N. Kikugawa, T. Kako, S. X. Ouyang, H. Stuart-Williams, H. Yang, J. Y. Cao, W. J. Luo, Z. S. Li, Y. Liu, R. L. Withers, *Nat. Mater.* **2010**, *9*, 559 – 564; d) L. W. Zhang, C. Y. Lin, V. K. Valev, E. Reisner, U. Steiner, J. J. Baumberg, *Small* **2014**, *10*, 3970 – 3978; e) B. Z. Tian, T. T. Wang, R. F. Dong, S. Y. Bao, F. Yang, J. L. Zhang, *Appl. Catal. B* **2014**, *147*, 22 – 28; f) A. Paracchino, V. Laporte, K. Sivula, M. Grätzel, E. Thimsen, *Nat. Mater.* **2011**, *10*, 456 – 461.

[2] a) J. Tian, Y. H. Sang, G. W. Yu, H. D. Jiang, X. N. Mu, H. Liu, *Adv. Mater.* **2013**, *25*, 5075 – 5080; b) A. L. Linsebigler, G. Lu, J. T. Yates Jr. , *Chem. Rev.* **1995**, *95*, 735 – 758; c) J. S. Zhang, M. W. Zhang, R. Q. Sun, X. C. Wang, *Angew. Chem. Int. Ed.* **2012**, *51*, 10145 – 10157; *Angew. Chem.* **2012**, *124*, 10292 – 10296.

[3] a) F. E. Osterloh, *Chem. Mater.* **2008**, *20*, 35 – 54; b) K. Maeda, K. Domen, *Chem. Mater.* **2010**, *22*, 612 – 623.

[4] a) K. Maeda, K. Domen, *J. Phys. Chem. Lett.* **2010**, *1*, 2655 – 2661; b) Y. S. Jun, J. Park, S. U. Lee, A. Thomas, W. H. Hong, G. D. Stucky, *Angew. Chem. Int. Ed.* **2013**, *52*, 11083 – 11087; *Angew. Chem.* **2013**, *125*, 11289 – 11293; c) P. Niu, L. L. Zhang, G. Liu, H. M. Cheng, *Adv. Funct. Mater.* **2012**, *22*, 4763 – 4770; d) Z. Z. Lin, X. C. Wang, *Angew. Chem. Int. Ed.* **2013**, *52*, 1735 – 1738; *Angew. Chem.* **2013**, *125*, 1779 – 1782.

[5] a) J. Xu, L. W. Zhang, R. Shi, Y. F. Zhu, *J. Mater. Chem. A* **2013**, *1*, 14766 – 14772; b) Y. Hou, Z. H. Wen, S. M. Cui, X. R. Guo, J. H. Chen, *Adv. Mater.* **2013**, *25*, 6291 – 6297; c) X. C. Wang, S. Blechert, M. Antonietti, *ACS Catal.* **2012**, *2*, 1596 – 1606.

[6] a) X. C. Wang, K. Maeda, A. Thomas, K. Takanabe, G. Xin, J. M. Carlsson, K. Domen, M. Antonietti, *Nat. Mater.* **2009**, *8*, 76 – 80; b) X. C. Wang, K. Maeda, X. F. Chen, K. Takanabe, K. Domen, Y. D. Hou, X. Z. Fu, M. Antonietti, *J. Am. Chem. Soc.* **2009**, *131*, 1680 – 1681; c) J. S. Zhang, X. F. Chen, K. Takanabe, K. Maeda, K. Domen, J. D. Epping, X. Z. Fu, M. Antonietti, X. C. Wang, *Angew. Chem. Int. Ed.* **2010**, *49*, 441 – 444; *Angew. Chem.* **2010**, *122*, 451 – 454.

[7] S. C. Yan, S. B. Lv, Z. S. Li, Z. G. Zou, *Dalton Trans.* **2010**, *39*, 1488 – 1491.

[8] L. Ge, C. C. Han, J. Liu, *Appl. Catal. B* **2011**, *108 – 109*, 100 – 107.

[9] S. Kumar, T. Surendar, A. Baruah, V. Shanker, *J. Mater. Chem. A* **2013**, *1*, 5333 – 5340.

[10] J. G. Yu, W. G. Wang, B. Cheng, *Chem. Asian J.* **2010**, *5*, 2499 – 2506.

[11] H. G. Kim, P. H. Borse, W. Y. Choi, J. S. Lee, *Angew. Chem.* **2005**, *117*, 4661 – 4665.

[12] L. R. Zheng, Y. H. Zheng, C. Q. Chen, Y. Y. Zhan, X. Y. Lin, Q. Zheng, K. M. Wei, J. F. Zhu, *Inorg. Chem.* **2009**, *48*, 1819 – 1825.

[13] P. Chen, L. Gu, X. B. Cao, *CrystEngComm* **2010**, *12*, 3950 – 3958.

[14] a) J. S. Zhang, G. G. Zhang, X. F. Chen, S. Lin, L. Möhlmann, G. Dołęga, G. Lipner, M. Antonietti, S. Blechert, X. C. Wang, *Angew. Chem. Int. Ed.* **2012**, *51*, 3183 – 3187; *Angew. Chem.* **2012**, *124*, 3237 – 3241; b) Y. J. Zhang, A. Thomas, M. Antonietti, X. C. Wang, *J. Am. Chem. Soc.* **2009**, *131*, 50 – 51.

[15] a) Y. J. Cui, Z. X. Ding, X. Z. Fu, X. C. Wang, *Angew. Chem. Int. Ed.* **2012**, *51*, 11814 – 11818; *Angew. Chem.* **2012**, *124*, 11984 – 11988; b) X. F. Chen, Y. S. Jun, K. Takanabe, K. Maeda, K. Domen, X. Z. Fu, M. Antonietti, X. C.

Wang, *Chem. Mater.* **2009**, *21*, 4093 – 4095; c) E. Z. Lee, Y. S. Jun, W. H. Hong, A. Thomas, M. M. Jin, *Angew. Chem. Int. Ed.* **2010**, *49*, 9706 – 9710; *Angew. Chem.* **2010**, *122*, 9900 – 9904.

[16] a) J. S. Zhang, M. W. Zhang, C. Yang, X. C. Wang, *Adv. Mater.* **2014**, *26*, 4121 – 4125; b) S. Zhou, Y. Liu, J. M. Li, Y. J. Wang, G. Y. Jiang, Z. Zhao, D. X. Wang, A. J. Duan, J. Liu, Y. C. Wei, *Appl. Catal. B* **2014**, *158 – 159*, 20 – 29.

[17] a) S. Wang, D. Li, C. Sun, S. Yang, Y. Guan, H. He, *Appl. Catal. B* **2014**, *144*, 885 – 892; b) H. P. Li, J. Y. Liu, W. G. Hou, N. Du, R. J. Zhang, X. T. Tao, *Appl. Catal. B* **2014**, *160 – 161*, 89 – 97.

[18] Y. Wang, H. R. Li, J. Yao, X. C. Wang, M. Antonietti, *Chem. Sci.* **2011**, *2*, 446 – 450.

[19] J. S. Zhang, M. W. Zhang, G. G. Zhang, X. C. Wang, *ACS Catal.* **2012**, *2*, 940 – 948.

[20] a) X. F. Gao, W. T. Sun, Z. D. Hu, G. Ai, Y. L. Zhang, S. Feng, F. Li, L. M. Peng, *J. Phys. Chem. C* **2009**, *113*, 20481 – 20485; b) S. Y. Chai, Y. J. Kim, W. I. Lee, *J. Electroceram.* **2006**, *17*, 909 – 912; c) D. W. Kim, S. Lee, H. S. Jung, J. Y. Kim, H. Shin, K. S. Hong, *Int. J. Hydrogen Energy* **2007**, *32*, 3137 – 3140; d) S. J. Hong, S. Lee, J. S. Jang, J. S. Lee, *Energy Environ. Sci.* **2011**, *4*, 1781 – 1787.

[21] a) T. Kawahara, Y. Konishi, H. Tada, N. Tohge, J. Nishii, S. Ito, *Angew. Chem. Int. Ed.* **2002**, *41*, 2811 – 2813; *Angew. Chem.* **2002**, *114*, 2935 – 2937; b) V. Etacheri, M. K. Seery, S. J. Hinder, S. C. Pillai, *Chem. Mater.* **2010**, *22*, 3843 – 3853; c) J. Zhang, Q. Xu, Z. C. Feng, M. J. Li, C. Li, *Angew. Chem. Int. Ed.* **2008**, *47*, 1766 – 1769; *Angew. Chem.* **2008**, *120*, 1790 – 1793.

[22] Z. X. Pei, L. Y. Ding, M. L. Lu, Z. H. Fan, S. X. Weng, J. Hu, P. Liu, *J. Phys. Chem. C* **2014**, *118*, 9570 – 9577.

[23] a) Y. Pihosh, I. Turkevych, K. Mawatari, T. Asai, T. Hisatomi, J. Uemura, M. Tosa, K. Shimamura, J. Kubota, K. Domen, T. Kitamori, *Small* **2014**, *10*, 3692 – 3699; b) Y. J. Cui, J. S. Zhang, G. G. Zhang, J. H. Huang, P. Liu, M. Antonietti, X. C. Wang, *J. Mater. Chem.* **2011**, *21*, 13032 – 13039; c) Y. J. Cui, J. H. Huang, X. Z. Fu, X. C. Wang, *Catal. Sci. Technol.* **2012**, *2*, 1396 – 1402.

[24] L. M. Sun, X. Zhao, C. J. Jia, Y. X. Zhou, X. F. Cheng, P. Li, L. Liu, W. L. Fan, *J. Mater. Chem.* **2012**, *22*, 23428 – 23438.

[25] a) S. Kumar, A. Baruah, S. Tonda, B. Kumar, V. Shanker, B. Sreedhar, *Nanoscale* **2014**, *6*, 4830 – 4842; b) H. Q. Li, Y. M. Cui, W. S. Hong, B. L. Xu, *Chem. Eng. J.* **2013**, *228*, 1110 – 1120.

[26] a) Z. Alferov, *Semiconductors* **1998**, *32*, 1 – 14; b) J. Tersoff, *Phys. Rev. B* **1984**, *30*, 4874 – 4877.

[27] a) C. Piliego, M. A. Loi, *J. Mater. Chem.* **2012**, *22*, 4141 – 4150; b) M. Muntwiler, Q. Yang, X. Zhu, *J. Electron Spectrosc. Relat. Phenom.* **2009**, *174*, 116 – 124.

[28] a) G. T. Li, K. H. Wong, X. Zhang, C. Hu, J. C. Yu, R. C. Chan, P. K. Wong, *Chemosphere* **2009**, *76*, 1185 – 1191; b) L. S. Zhang, K. H. Wong, H. Y. Yip, C. Hu, J. C. Yu, C. Y. Chan, P. K. Wong, *Environ. Sci. Technol.* **2010**, *44*, 1392 – 1398; c) M. C. Yin, Z. S. Li, J. H. Kou, Z. G. Zou, *Environ. Sci. Technol.* **2009**, *43*, 8361 – 8366; d) N. Zhang, S. Q. Liu, X. Z. Fu, Y. J. Xu, *J. Phys. Chem. C* **2011**, *115*, 9136 – 9145; e) U. F. Alkaram, A. A. Mukhlis, A. H. Al-Dujaili, *J. Hazard. Mater.* **2009**, *169*, 324 – 332; f) H. Q. Li, W. S. Hong, Y. M. Cui, Q. F. Jia, S. H. Fan, *J. Mol. Catal. A* **2013**, *378*, 164 – 173.

[29] a) S. H. Yoon, J. H. Lee, *Environ. Sci. Technol.* **2005**, *39*, 9695 – 9701; b) S. C. Yan, Z. S. Li, Z. G. Zou, *Langmuir* **2010**, *26*, 3894 – 3901.

[30] J. Fu, B. B. Chang, Y. L. Tian, F. N. Xi, X. P. Dong, *J. Mater. Chem. A* **2013**, *1*, 3083 – 3090.

Received: January 7, 2015
Published online on February 26, 2015